Chapter 3

Experimental techniques

3.1 Sample synthesis and thermal treatment

3.1.1 Synthesis method: arc melting

The method used in this work to synthesize the samples of the $Gd_5(Si_xGe_{1-x})_4$ series of alloys is arc melting, a simple but effective method. The process consists in melting the pure elements of the alloy in the desired stochiometry by discharging an electrical arc due to the application of a large tension between two electrodes. Our arc-melting furnace was designed and constructed in the mechanical workshop of Facultat de Física of the Universitat de Barcelona, specifically to prepare bulk intermetallic alloys, *i.e.*, it is not a commercial furnace (see Figs. 3.1 and 3.2). The power (current) supply is a TIG 160 AC/DC (Argon), which may supply up to 160 A. The anode, which lies over a steel platform, is a Cu crusible designed to hold the samples of the pure elements. It is cooled by a water flow to avoid heating and melting of the Cu. The platform is covered by an hermetical cylinder of stainless steel, which holds the cathode in its inner top. The cathode consists in a sharp rod of W -with 2% of Th-, a refractory material that bears high temperatures without melting. The cover enables to control the atmosphere of the furnace chamber by flowing high-purity Ar, which evacuates oxygen and act as ionizing gas.

The procedure to synthesize a sample is summarised as follows: after the tension is applied, the cathode is approached to the pure elements that are placed on the Cu crusible, by turning a millimetric screw. Argon gas must flow through the furnace chamber at a pressure of 1-1.5 bar. When the cathode is close enough, an arc that melts the elements is discharged by ionizing the gas. After some seconds of melting, the pure elements are mixed and the tension can be broken off. The synthesis process of a sample includes a number of meltings, with the sample being turned over each time in order to ensure a good homogeneity of the elements

Figure 3.1: Complete view of the arc-melting furnace: chamber, power supply and Ar gas cylinder.

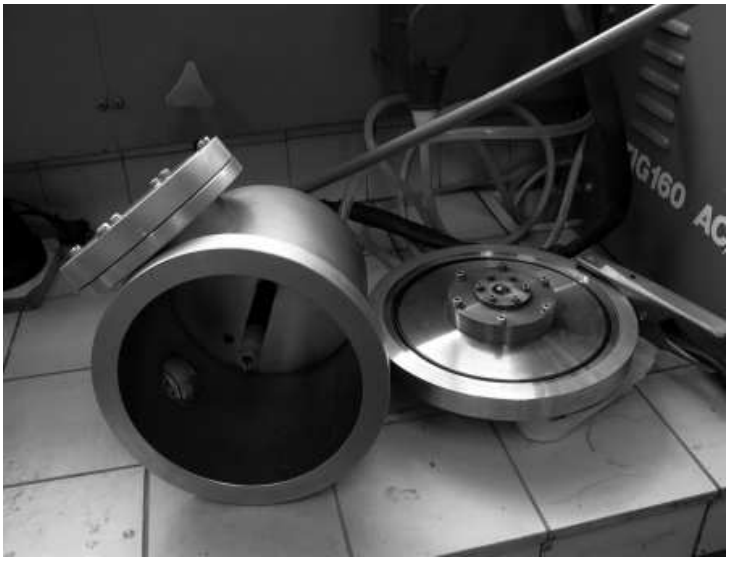

Figure 3.2: Detail of the inside of the arc-melting furnace chamber: cover with the cathode, on the left, and water-cooled Cu crusible (anode) with a sample above, on the right.

in the alloy. The sample is weighted after each melting to control possible weight losses, which must be negligible to maintain the desired stochiometry. At least one of the elements must be metallic, because on the contrary the arc can not be discharged.

Alloys are easy to obtain with this method, but it also presents a drawback: sample cooling is not homogeneous when the arc is broken off. At the bottom of the sample, where there is contact with the water-cooled Cu crusible, the cooling of the sample is faster than at the top of the latter. This fact can be observed in the shape of as-prepared samples of $Gd_5(Si_xGe_{1-x})_4$ alloys. During the brief cooling process, the top sample crystallises forming characteristic faceted -and bright- sides, like a football ball. At the bottom, the alloy does not cristallise in facets and it simply presents a metallic look.

Samples of $Gd_5(Si_xGe_{1-x})_4$ obtained in this work generally have a mass between 1 and 2 g, and a current of ~80 A is needed to melt them. It is worth noting that these samples are quite brittle and usually display cracks (the more Ge content, the more brittle), so that cutting the samples to obtain fragments for their characterisation presents some problems[1]. Table 3.1 display all synthesized samples with their partitions, and the further heat treatments and measurements carried out over them. All in all, almost 50 samples have been studied. Since this work is aimed at the study of MCE at the first-order transition of $Gd_5(Si_xGe_{1-x})_4$ alloys, the synthesized samples lies within the compositional range $0 \leq x \leq 0.5$.

3.1.2 Heat treatment

When a sample of $Gd_5(Si_xGe_{1-x})_4$ with the desired stochiometry is synthesized, some phases with a different value of x may appear due to segregation processes. This is critical for compositions close to the boundary of compositional regions ($x \cong 0.5$, $x \cong 0.2 - 0.24$), because residual phases with distributed value of x -*i.e.*, with different structures and magnetic ordering- can be present (see section 2.2 and Ref. [1]). Secondary phases as $Gd_5(Si,Ge)_3$ (5:3) and Gd(Si,Ge) (1:1) may appear [2, 3, 4], since they are close to $Gd_5(Si,Ge)_4$ (5:4) in composition ratio. This is evident from the Gd-Ge and Gd-Si phase diagrams displayed in Figs. 3.3 and 3.4. A proper heat treatment should removes the residual 5:4 phases with distributed value of x [1], because it would help to homogenise Si and Ge content all over the sample. However, a high-temperature polymorphic transformation for $x \cong 0.5$ compounds has very recently been found (see section 2.2), leading to the the formation of the $O(I)$ phase from the room-temperature M phase. The polymorphism is irreversible between ~500 K and ~870 K [5, 6, 7, 8], therefore a heat treatment up to those temperatures would change the structure of the phase

[1] To avoid breaking of the sample, a low-speed saw has always been used.

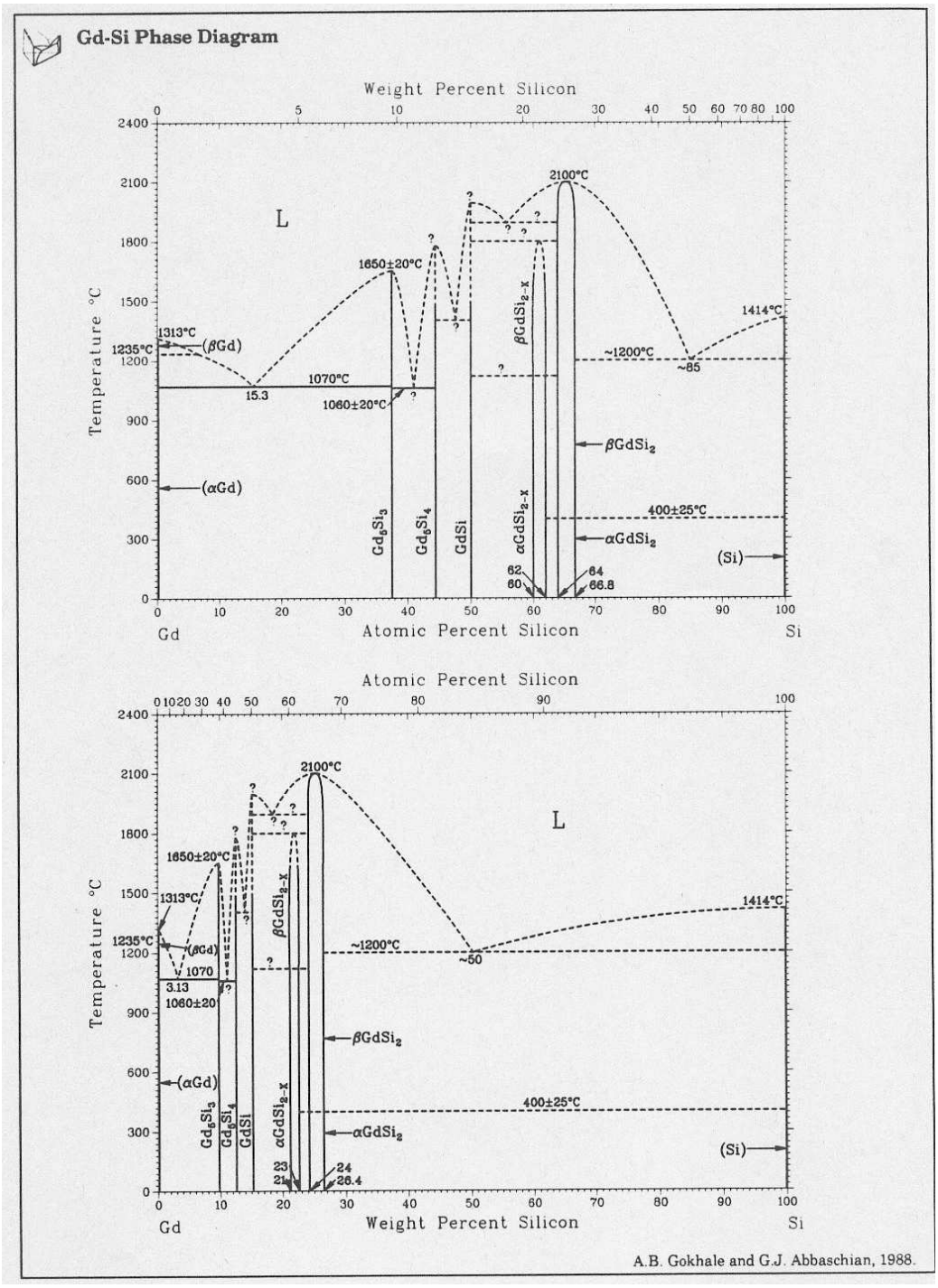

Figure 3.3: Gd-Si phase diagram as a function of atomic percent silicon (upper panel) and weight percent silicon (lower panel).

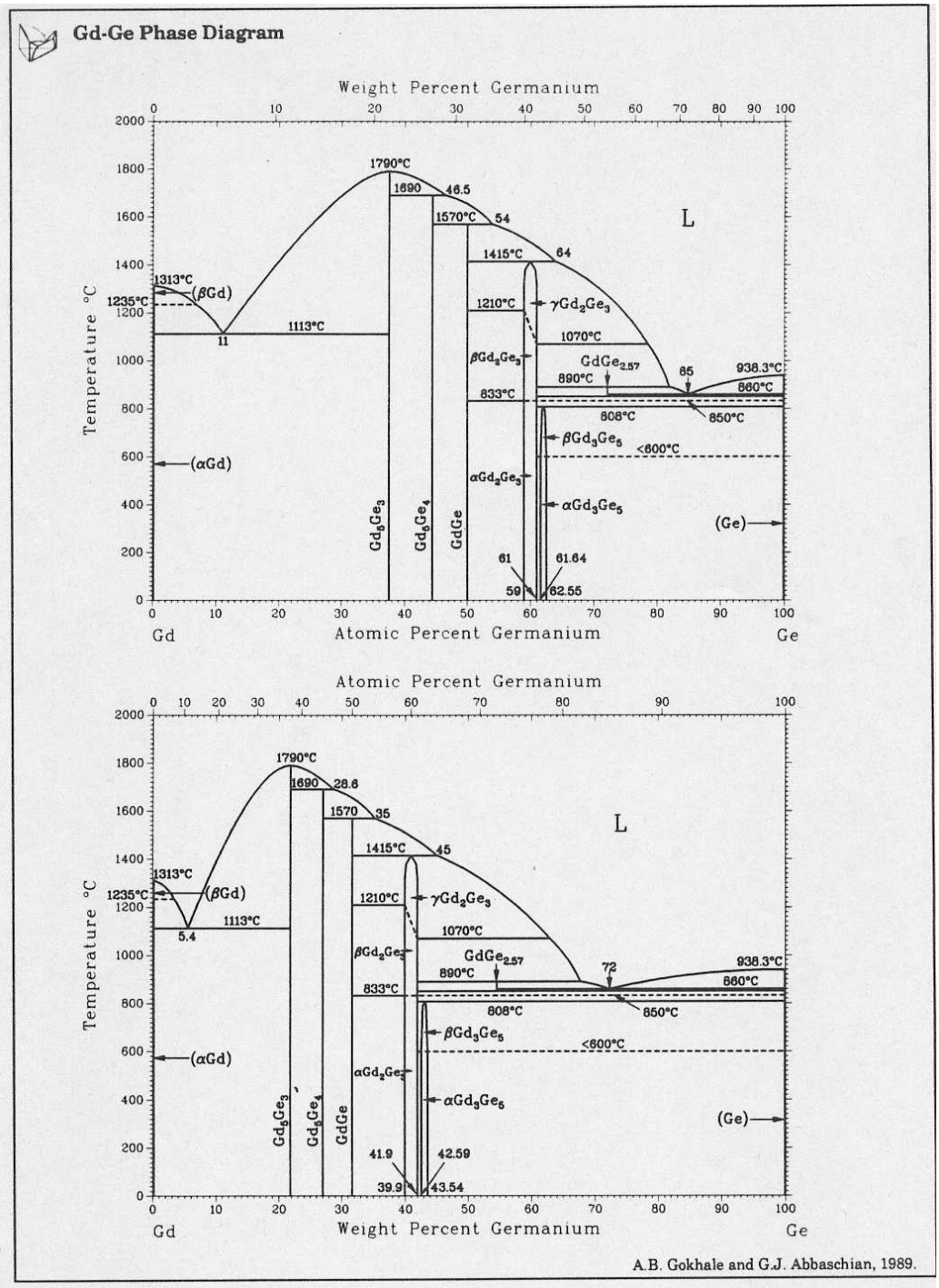

Figure 3.4: Gd-Ge phase diagram as a function of atomic percent germanium (upper panel) and weight percent germanium (lower panel).

and the MCE. This transformation becomes reversible at ~1070 K and, at least, up to 1570 K [2] [5, 6, 7]. With all these considerations, we tried to find the best heat treatment for as-cast samples. After each heat treatment, samples where analised by various magnetic and structural characterisation techniques (which are described in section 3.2). The efficiency of each heat treatment is also discussed in section 3.2. The variety of thermal treatments used are the following:

(i) T1. 4 hours at 1400 ºC under a pure Ar flow, as mentioned in Ref. [1], with a heating/cooling rate of 5º/min. from/to room temperature in a ceramic tubular furnace. A sample holder of alumina was used in order to bear this temperature. We already noted that the appearance of the samples proved an evident oxidation, with a white powder covering them (gadolinium oxide Gd_2O_3 shows this aspect). Degasing of alumina may be responsible of the oxidation for the samples.

(ii) T2. We repeated the same treatment (4 hours at 1400ºC) but adding 0.5% of H_2 in the gas flow -which is a reductor gas- to avoid the oxidation. The appearance of the samples was much better: although the surface seemed oxidised, the inside of the samples looked completely metallic.

(iii) T3. This heat treatment was the same as T2, but with the annealing temperature lowered to 1000 ºC, in order to study the effect of T in the heat-treated samples.

(iv) T4. Since it was suspected that the oxidation came from either impurities of Ar (unlikely) or degasing of alumina sample holder (likely), we used an electrical resistance furnace: samples were placed in a quartz tube (which does not degas but bears lower temperatures than alumina) under a vacuum of 10^{-5} mb, and heated at 50º/min up to 950 ºC for 4 hours. Afterwards, the resistance was switched off and cooling to room temperature lasted ~1 hour. The appearance of the samples was darker than as-cast ones, but without sign of oxidation.

(iv') T4+Q. This heat treatment is very similar to T4, using the same furnace with a quartz tube to reach a high vacuum (10^{-5} mb). In this case, samples were annealed up to 920 ºC for 8h 45' and, after annealing, the quartz tube was quickly taken out of the furnace to room temperature (quenching).

(v) T5. To reach higher annealing temperatures, we repeated the heat treatment in the ceramic furnace used in T1, T2 and T3, by replacing the alumina sample holder for a platinum wire, which should also bear high temperatures but does not degas, as alumina does. After annealing at 1400ºC for 4 hours, Pt was destroyed. Silicon of the samples diffused to Pt, whose structure was completely damaged. Obviously, samples were also damaged.

[2] A $M \leftrightarrow O(I)$ transition thus exists between ~870 K and ~1070 K, see section 2.2.

3.1. Sample synthesis and thermal treatment

x	ID	heat t.	partition		XRD	SEM	MR	ac	DSC	M(H)	M(T)	dscH
0	#1	NO	$\frac{1}{2}$	rod 1		X				X	X	
				rod 2		X						$\dot{T}$
				powder	X							
		T5	$\frac{1}{2}$									
0	#3	NO		powder	X							
0.05	#1	T4+Q	$\frac{1}{2}$	rod 1								$\dot{H}$
				rod 2								$\dot{H}$
			$\frac{1}{2}$	rod 1b								$\dot{H}$
				rod 2b						X	X	$\dot{T}/\dot{H}$
0.1	#1	NO	$\frac{1}{2}$	rod 1								
				rod 2						X		$\dot{T}/\dot{H}$
				powder	X							
		T5	$\frac{1}{2}$									
0.15	#0	NO		pressed			X					
0.15	#1	NO/T1		piece				X/	X/X			
		NO/T1		rod				X/X				
0.18	#1	T2	$\frac{1}{4}$	rod 1								
				rod 2								
		T3	$\frac{1}{4}$									
		NO	$\frac{1}{4}$	rod 1				X	X	X		
				rod 2								
		T4	$\frac{1}{4}$	rod 1				X	X	X		$\dot{T}$
				rod 2				X				
0.2	#1	NO	$\frac{1}{2}$	rod 1					X			$\dot{T}$
				rod 2		X				X		
				powder	X							
		T5	$\frac{1}{2}$									
0.25	#2	NO	$\frac{1}{2}$	rod 1					X			$\dot{T}$
				rod 2								
0.3	#2	NO	$\frac{1}{2}$	rod 1					X			$\dot{T}$
				rod 2 (powd.)	(X)							
		T4+Q	$\frac{1}{2}$	rod 1						X		$\dot{T}/\dot{H}$
				rod 2								

x	ID	heat t.	partition		XRD	SEM	MR	ac	DSC	M(H)	M(T)	dscH
0.365	#1	NO/T1		piece				X/	X/X			
		NO/T1		rod				X/X				
		NO		slice Cu			X					
0.365	#2	T2	$\frac{1}{3}$									
			$\frac{2}{3}$	rod					X			
0.365	#3	NO	$\frac{1}{2}$	rod 1					X	X		
				rod 2								$\dot{T}$
		T5	$\frac{1}{2}$									
0.45	#0	NO	1	slice A	X		X					
				slice B			X					
0.45	#1	NO		slice C			X					
		NO		slice D	X							
		NO/T1		piece				X/	X/X			
0.45	#2	NO/T1		slice E	X/							
		T1		slice F			X					
0.45	#4	NO	$\frac{1}{2}$				X					
		NO	$\frac{1}{2}$				X					
0.45	#5	T2		rod 1				X	X	X		
				rod 2								
				powder	X							
0.45	#7	T2	$\frac{1}{4}$									
		T3	$\frac{1}{4}$	rod 1						X		
				rod 2								
		NO	$\frac{1}{4}$	rod 1 (powd.)	(X)			X	X	X		$\dot{T}$
				rod 2		X						$\dot{T}$
		T4	$\frac{1}{4}$	rod 1 (powd.)	(X)			X	X	X		$\dot{T}/\dot{H}$
				rod 2		X						
		T4+Q	piece	powder	X							
0.5	#0	NO		powder	X							

Table 3.1: Detail of all samples synthesized. x is the composition of the $Gd_5(Si_xGe_{1-x})_4$ sample. ID stands for an identification number for each sample with the same x. Heat treatments: no heat treatment (NO), T1, T2, T3, T4, T4+Q and T5 (see text for details). Partition explains the fractions of a given sample and their shapes. Measurements done: X-Ray diffraction (XRD), scanning electron microscopy and microprobe (SEM), magnetoresistance (MR), ac susceptibility (ac), differential scanning calorimetry (DSC), magnetisation (M(H) and M(T)) and DSC under magnetic field (dscH). $\dot{T}$ stands for measurement sweeping T and $\dot{H}$ sweeping H.

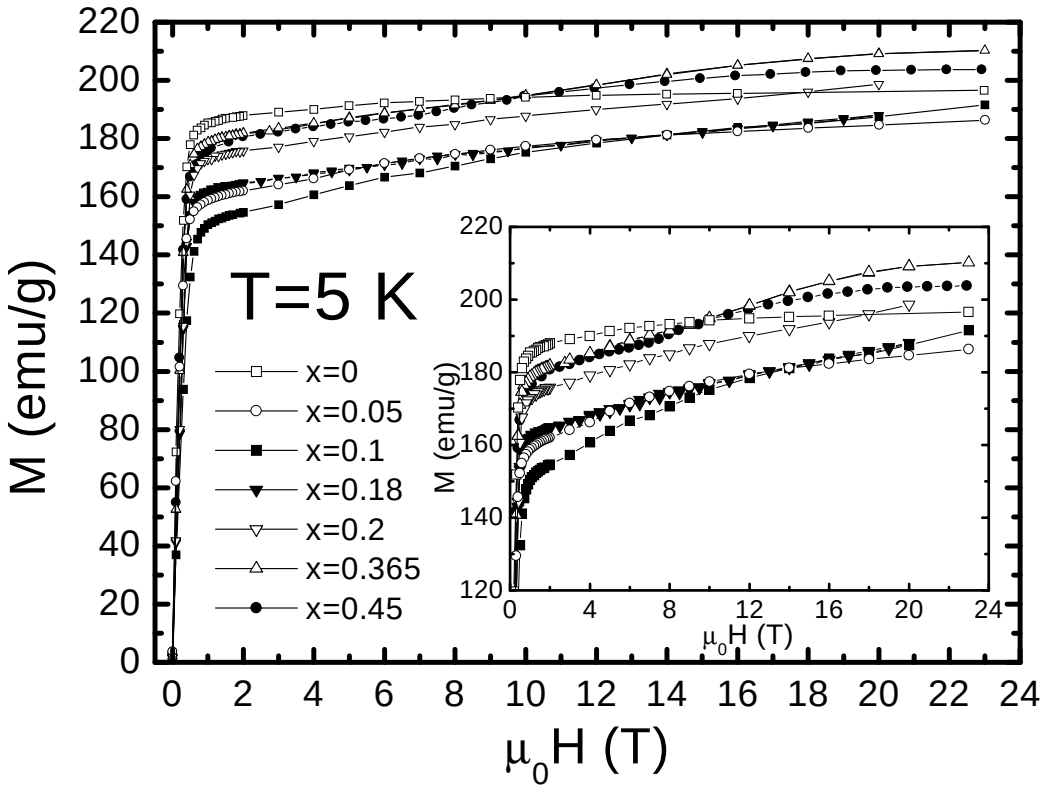

Figure 3.5: Magnetisation isotherms at 5 K for the following as-cast samples: x= 0, 0.05, 0.1, 0.18, 0.2, 0.365 and 0.45. Inset: Detail of the isotherms.

3.2 Sample characterisation

3.2.1 Magnetisation

Magnetisation measurements were mostly carried out at the Grenoble High Magnetic Field Laboratory (GHMFL), which is managed by CNRS and MPI-FKF. An extraction magnetometer operating from 4.2 to 325 K (using a dynamic He cryostat) and up to 23 T (using a 10 MW resistive magnet) was used. The first measurement performed for each sample before the systematic study of the first-order field-induced magnetic phase transition (see section 5.2) was $M(H)$ at 5 K. These magnetisation curves are displayed in Fig. 3.5 for a variety of as-cast samples (x=0, 0.05, 0.1, 0.18, 0.2, 0.365 and 0.45). All curves show a large high-field magnetic susceptibility. The ordered magnetic moment, extrapolated to zero magnetic field, is displayed in Table 3.2 along with values obtained from the literature. The theoretical value of the ordered magnetic moment at the saturation for a free Gd^{3+} ion is 7.0 μ_B and for metallic Gd is 7.56 μ_B. Isotherms for x=0, 0.365 and

x	M_S (μ_B/Gd at.) this work	literature
0	7.38	7.32 [9], 7.41 [10]
0.05	6.62	
0.0825		7.36 [10]
0.1	6.28	
0.18	6.18	
0.2	6.55	
0.2525		7.39 [10]
0.365	7.19	
0.375		7.05 [11, 12]
0.43		7.46 [10]
0.45	7.18	
0.5		7.36 [10]

Table 3.2: Ordered magnetic moment extrapolated at zero field from the saturation magnetisation at T=5 K, for as-cast samples with composition x. Some values given in literature are also included for comparison.

Compound	$T_N(K)$	θ_C (K)	p_{eff} (μ_B)	Crystal structure	Reference
Gd_5Ge_3	74/74	70/65	8.42/7.82	Mn_5Si_3-type hexagonal	[15]/[14]
Gd_5Si_3	-/55	97/42	8.34/8.5	Mn_5Si_3-type hexagonal	[15]/[14]
GdGe	62	-13	8.21	CrB-type orthorhombic	[15]
GdSi	50/56.2	5/-10.5	8.23/8.63	FeB-type orthorhombic	[15]/[13]

Table 3.3: Magnetic and structural properties of possible secondary phases present in $Gd_5(Si_xGe_{1-x})_4$ alloys. All phases are AFM. T_N stands for the Néel temperature, θ_C for the paramagnetic Curie temperature and p_{eff} for the effective magnetic moment.

0.45 show saturation after a change of slope at ~5, ~12, and ~9 T, respectively. Their saturation magnetisation exceeds the theoretical value by 0.2-0.4μ_B, probably due to the contribution of $6s$ and $5d$ electrons. The rest of the samples do not reach the saturation and also present a change of slope at ~4 T with a slight hysteresis. This fact evidences the presence of non-FM residual phases, different from the main 5:4 phase. The amount of these secondary phases depends on x, according to the values of the saturation moment. From the Gd-Si and Gd-Ge phase diagrams (Figs. 3.3 and 3.4), phases with 5:3 and 1:1 appear as the most likely. All these phases, whose properties are listed in Table 3.3, are AFM. Therefore, their magnetic behaviour could account for the slope of the high-field magnetisation isotherms, which is very large for both the 1:1 [13] and 5:3 [14] phases. Moreover, a spin-flop metamagnetic transition is reported for Gd_5Ge_3 and Gd_5Si_3 at fields of ~6.8 and 4.8 T, respectively [14], in concordance with the observed behaviour in our samples.

Magnetisation isotherms at 5 K can also be used to check possible effects of the heat treatments on the samples. Figure 3.6 shows $M(H)$ at 5 K for x=0.45 for the variety of heat treatments (as-cast, T2, T3 and T4). Measurement of the sample with T3 was carried out up to 5 T in a Quantum Design SQUID. Inset of Fig. 3.6 displays the same results for x=0.18 (as-cast and T4).

It is worth noting that samples with T2 and T3 treatments show the same curve, proving that annealing within 1000 and 1400ºC is not a key parameter. Saturation magnetisation is lowered ~30% and there is a larger slope in the latter annealed samples with respect to the as-cast sample, which evidences that a large part of the sample shows the appearance of an undesired phase, and/or the growing of a secondary phase already present in the sample, that saturates at ~10 T. For T4 treatment, the saturation is only reduced ~8% for x=0.45 (~12% for x=0.18). Therefore, although all heat treatments homogenise the x value of the 5:4 main

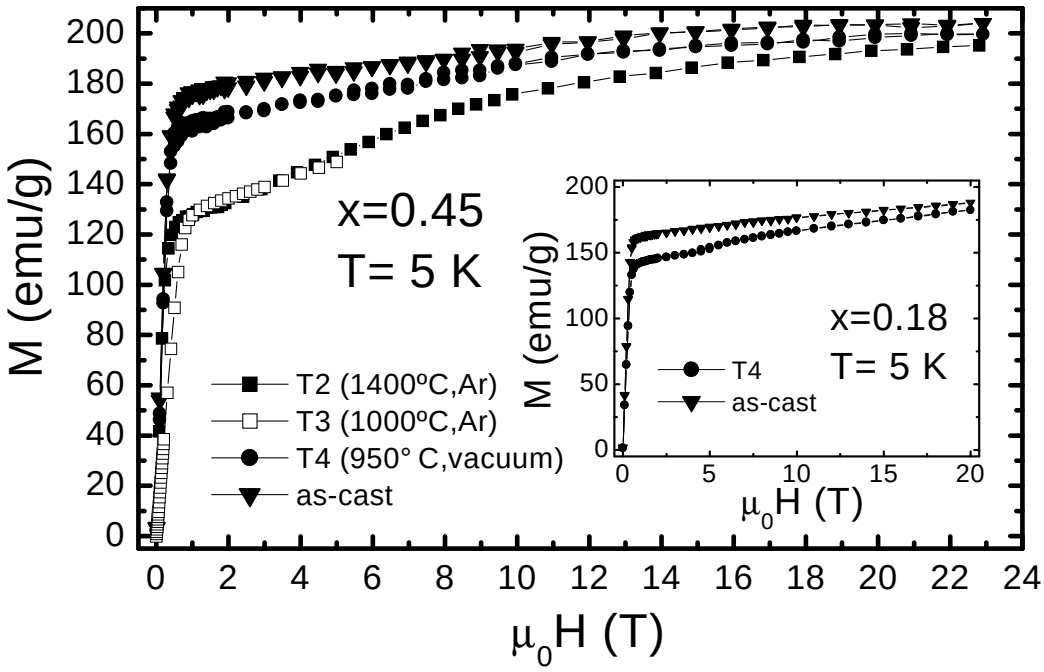

Figure 3.6: Magnetisation isotherms at 5 K for x=0.45 with different heat treatments (as-cast, T2, T3 and T4). Inset: Magnetisation isotherms at 5 K for x=0.18 (as-cast and T4).

phase (see sec. 3.2.2 -ac susceptibility-, sec. 3.2.3 -DSC- and sec. 3.2.4 -XRD-), they also yield the appearance of one or some undesired phases which are not FM at 5 K up to at least ~10 T) and this effect is lesser for the T4 treatment. However, these secondary phases do not affect the magnetism of the alloy.

3.2.2 Ac susceptibility

When a sample is exposed to an alternating magnetic field (with an angular frequency $\omega = 2\pi\nu$, being ν the linear frequency), written in complex notation as

$$H(t) = H_{\rm dc} + H_{\rm ac}\, e^{i\omega t} \quad , \tag{3.1}$$

the magnetisation in the stationary state will also exhibit a periodic time dependence with the same frequency ω

$$M(t) = H_{\rm dc}\chi_0 + H_{\rm ac}\chi_{\rm ac}\, e^{i\omega t - i\phi} \quad , \tag{3.2}$$

where ϕ denotes the phase difference between the applied magnetic field and the sample magnetisation. $\chi_0 (= M/H_{\rm dc})$ is the static susceptibility and it is not measured in ac experiments. The complex ac susceptibility $\overline{\chi} \equiv \chi_{\rm ac}\, \exp(-i\phi)$ can be decomposed in an in-phase component χ' and an out-of-phase component χ'',

$$\overline{\chi} \equiv \chi_{\rm ac}\, e^{-i\phi} = \chi' - i\chi'' \quad , \tag{3.3}$$

where the minus sign arises from the fact that χ'' is usually defined to be positive. If $H_{\rm ac}$ is sufficiently small, the measured module of the susceptibility $\chi_{\rm ac}$ is to a good degree equal to the so-called dynamic susceptibility $\partial M(H)/\partial H$. At zero dc field, the measured ac susceptibility is approximately equal to the dynamic initial susceptibility, $\lim_{H\to 0} \partial M(H)/\partial H$. Therefore, ac susceptibility is a suitable technique to observe the different magnetic transitions in a material, since it measures the response of the system to a magnetic field oscillation.

The field in the bulk of a magnetic sample differs from the applied field due to the existence of magnetic dipoles which appear at the sample surface and generate a field inside the sample that opposes to the external applied field. This field is known as the demagnetising field. Accordingly, the effective field inside the sample, $H_{\rm int}$, is

$$H_{\rm int} = H_{\rm ext} - DM \quad , \tag{3.4}$$

where $H_{\rm ext}$ is the external field, M the sample magnetisation, and D the demagnetisation factor, which depends on the sample's geometry. In *SI* units, D may adopt values within 0 and 1, while in *CGS* units, D varies between 0 and 4π. For a magnetic field applied along a cylinder of infinite lenght or in parallel to the surface of an infinite plane, then $D = 0$, whereas $D = 4\pi$ (or 1 in *SI*) when the

field is applied perpendicular to an infinite plane. In the special case of a sphere, D is equal to $4\pi/3$ (*CGS*) or $1/3$ (*SI*). For samples with an arbitrary geometry the calculation of the demagnetisation factors becomes a very complicated task [16, 17].

Susceptibility has to be calculated using H_{int} rather than H_{ext}. If the correct value of the susceptibility (calculated from H_{int}) is χ_{int} and the value that is measured assuming a magnetic field of H_{ext} is χ_{meas}, then

$$\chi_{\text{int}} = \frac{\chi_{\text{meas}}}{1 - D\chi_{\text{meas}}} \quad . \tag{3.5}$$

Since $\chi = \chi' - i\chi''$ is a complex quantity, the above correction takes the following form:

$$\chi'_{\text{int}} = \frac{\chi'_{\text{meas}}(1 - D\chi'_{\text{meas}}) - D\chi''_{\text{meas}}}{(1 - D\chi'_{\text{meas}})^2 + (D\chi''_{\text{meas}})^2} \;\; ; \;\; \chi''_{\text{int}} = \frac{\chi''_{\text{meas}}}{(1 - D\chi'_{\text{meas}})^2 + (D\chi''_{\text{meas}})^2} \quad . \tag{3.6}$$

It is useful to know under which conditions χ_{meas} will significantly differ from the real susceptibility χ_{int}. For this purpose, we express χ_{meas} in terms of χ_{int} by inverting Eq. 3.5, as

$$\chi_{\text{meas}} = \frac{1}{\frac{1}{\chi_{\text{int}}} + D} \quad . \tag{3.7}$$

It is clear from the above expression that $\chi_{\text{meas}} \approx \chi_{\text{int}}$ as long as $\chi_{\text{int}} \ll 1/D$. On the contrary, if χ_{int} is very large ($\chi_{\text{int}} \gg 1/D$), the measured susceptibility $\chi_{\text{meas}} \approx 1/D$ and is almost insensitive to any real variation of χ_{int}. Large χ_{int} can occur in ferromagnetic materials, and in this case, one should try to minimise the demagnetisation factor D, which can be done by cutting the sample to an appropriate shape, such as in the form of a thin plane or an elongated needle with their axis parallel to the applied field.

The equipment used to measure ac susceptibility in our samples is a Lake Shore 7000 series susceptometer/magnetometer, which operates from 77 to 300 K. The high magnetisation of $Gd_5(Si_xGe_{1-x})_4$ samples (up to 200 emu/g at saturation) gives rise to a high demagnetising field, hence a very small D value is desirable.

After first measurements, we observed that D was too large and that the demagnetising field overlapped the results, even after the correction. Therefore, the new samples were cut as long rods, to minimise D. Although the shape of the rods is similar to a prism, calculation of D was approached by using the formula of a prolate spheroid when the field is applied along its longer dimension, c [18]:

$$D_c = \frac{4\pi}{r^2 - 1}\left[\frac{r}{\sqrt{r^2 - 1}} ln\left(r + \sqrt{r^2 - 1}\right) - 1\right] \quad (CGS) \;\; , \tag{3.8}$$

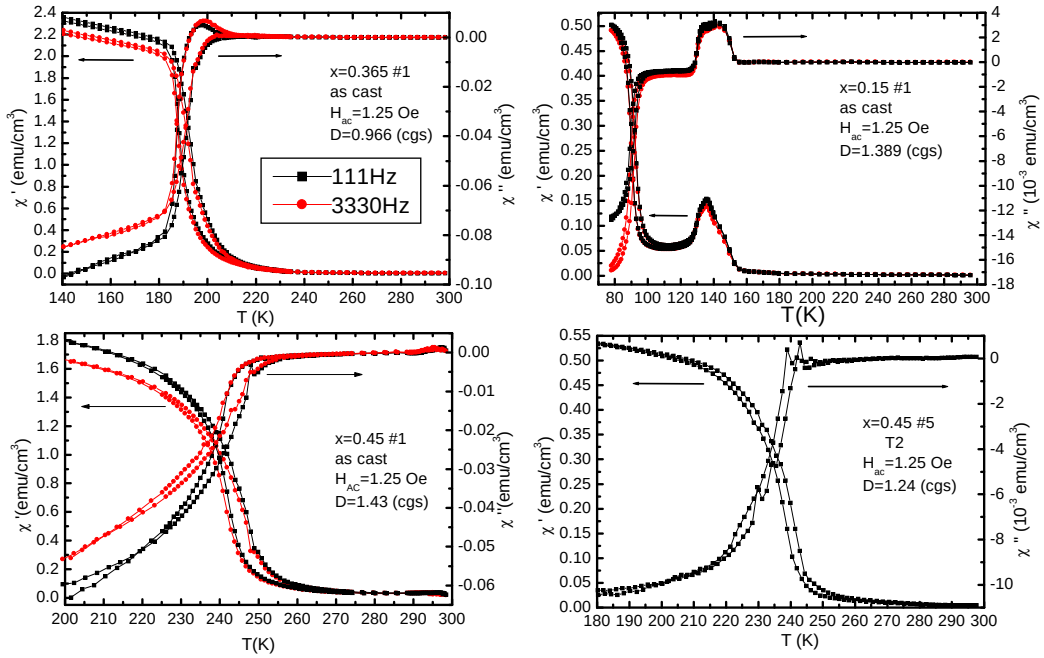

Figure 3.7: Real and imaginary part of the ac susceptibility, for x=0.15 (#1), x=0.365 (#1) and x=0.45 (#1) as-cast samples, and for x=0.45 (#5) T2-heat-treated sample. Frequencies ν=111 Hz (black squares) and 3330 Hz (red spheres) were applied in nule dc field and ac field of 1.25 Oe. Demagnetising field was corrected using the value of D labeled for each sample and calculated from Eq. 3.8.

being $a = b < c$ and $r = c/a$. Measurements were performed at zero dc field, ac field of 1.25 Oe, and frequencies ν=111 and 3330 Hz. First as-cast samples -x=0.15 (#1), 0.365 (#1) and 0.45 (#1)- were measured (see Fig. 3.7) to check whether the arc-melting furnace yielded a correct synthesis. The expected magnetic transitions in literature were used as the test to check the quality of the samples. Demagnetisation factors of the samples were D=1.389, 0.966 and 1.43 (*CGS*), respectively.

For x=0.45 (#1) as-cast sample (lower left panel in Fig. 3.7), the FM↔PM transition is observed in both χ' and χ''. The first-order nature is evident, since the transition spreads over a temperature range and thermal hysteresis is observed (T_t calculated at the point of maximum slope yields 245.9 K on heating and 241.3 K on cooling, in agreement with other authors [1, 10, 19]). The effect of frequency is only appreciable in the FM region, where the absolute values of both susceptibilities are lower at high frequency, as expected. A slight hysteresis of ~0.5-0.8 K occurs between both frequencies. At high temperatures (~297 K) an anomaly is observed, probably due to a residual phase with x>0.5, with a second-order

FM↔PM transition at that temperature [1]. It is worth noting the negative value of χ" in the FM phase, vanishing to zero at the transition to the PM phase. χ" is proportional to the energy absorbed in the system from the ac magnetic field and is thus defined as positive. This unusual behaviour, observed in all $Gd_5(Si_xGe_{1-x})_4$ samples, is believed to be caused by either the anomalous relaxation processes of the domain-wall motion and/or the excitation to a nonequilibrium state due to the external field [11].

For x=0.365 (#1) as-cast sample (upper left panel in Fig. 3.7) the same behaviour as that for x=0.45 sample is observed. In this case, T_t=188.4 K (193.0 K) on cooling (heating), in agreement with other authors [11, 20] and the phase diagram (Fig. 2.2). No anomalies due to residual phases are observed. Hysteresis in frequency is ~1 K.

For x=0.15 (#1) as-cast sample (upper right panel in Fig. 3.7), two transitions are observed, as it is expected for the $x \leq 0.2$ compositional region. The first-order magnetostructural FM↔AFM transition occurs at T_t=90 K (92 K) on cooling (heating), with a negligible hysteresis in frequency. At T_N=135.6 K (without either thermal or frequency hysteresis), the second-order AFM↔PM magnetic transition takes place, giving rise to a high susceptibility. In this case, the imaginary part of the susceptibility is negative in the FM region, it becomes smaller but still negative in the AFM phase, it changes to a positive value at the second-order transition region, and finally tends towards zero at the PM phase.

Therefore, samples within the different compositional regions can be successfully prepared with our arc-melting furnace. After this first conclusion, ac susceptibility for a sample x=0.45 (#5) with a T2 thermal treatment was measured (lower right panel in Fig. 3.7) in order to check the effect of the heat treatments on the transitions. For this sample, D=1.24 (CGS). T_t appears at 237.5 K (240.0 K) on cooling (heating), values very close to those given in Ref. [1], in which the sample was similarly heat-treated. The temperature spread in which the transition takes place is reduced, showing a more abrupt jump, which is an indication that x distribution around the stochiometric value is narrowed. Thermal hysteresis is also reduced. The high temperature anomaly disappears, showing that this heat treatment removes most of 5:4 residual phases with x departuring from nominal value, in spite of the damage caused to the sample observed in magnetisation measurements (section 3.2.1).

Since the magnetisation measurements already showed that the T4 treatment was better than the T2 treatment, a detailed study of ac susceptibility for the as-cast and T4 heat-treated samples was carried out. In order to analyse the $0.24 \leq x \leq 0.5$ region, a new x=0.45 sample (#7) was arc-melted and cut, and a part of it was annealed according to T4. Samples were rod-shaped to minimise the demagnetising field, with D=1.82 and 1.13 (CGS) for as-cast and heat-treated samples, respectively. In this case, the main differences already observed between

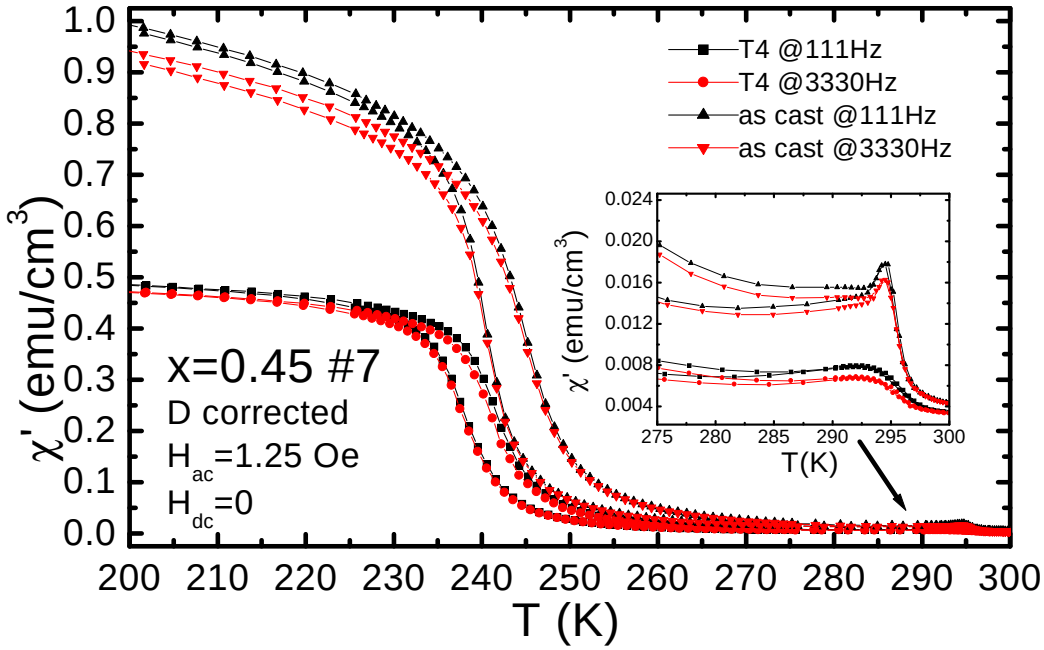

Figure 3.8: Real part of the ac susceptibility, for x=0.45 (#7) as-cast and heat-treated (T4) samples. Frequencies ν=111 Hz and 3330 Hz were used in nule dc field and ac field of 1.25 Oe. Demagnetising field was corrected. Inset: detail of the signal at high temperature, evidencing the anomaly present in as-cast sample, which is reduced in the heat-treated sample.

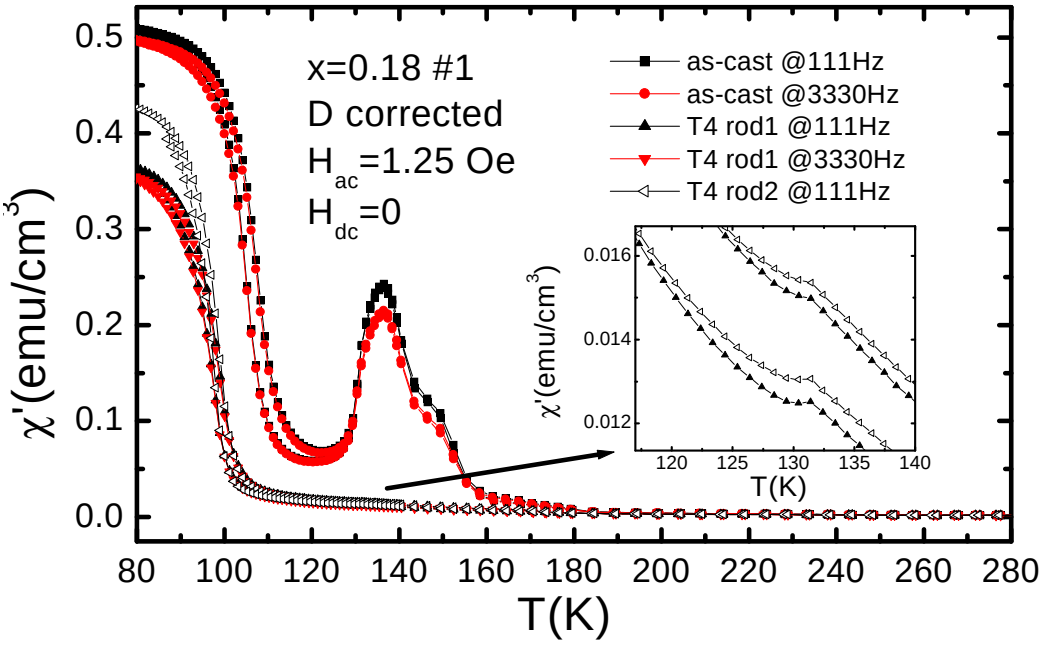

Figure 3.9: Real part of the ac susceptibility, for x=0.18 (#1) as-cast and heat-treated (T4) samples. Frequencies ν=111 Hz and 3330 Hz were used in nule dc field and ac field of 1.25 Oe. Demagnetising field was corrected. Inset: detail of the signal of the heat-treated sample near the second-order transition.

x=0.45 (#1) as-cast and x=0.45 (#5) T2 samples appeared again (see Fig. 3.8): (i) Signal in the FM phase is reduced in the heat-treated sample, evidencing an increase in the magnetic correlations in the latter; (ii) the transition on cooling (heating) is tuned from 240.7 (245.2) K to 239.3 (241.1) K, being sharper and with less thermal hysteresis for the T4-treated sample with respect to the as-cast one; and (iii) the anomaly which appears in the as-cast sample at high temperature (T=294.5±0.5 K, *i.e.*, a residual phase with x ~0.51-0.53 [1, 21]) is considerably reduced in the heat-treated sample (inset in Fig. 3.8).

The latter study was repeated within the $x \leq 0.2$ region, using x=0.18 (#1) sample, which was cut in 3 rods and two of them were annealed (T4). Figure 3.9 displays ac susceptibility for as-cast and annealed samples, where the demagnetising field has been corrected (D=1.27, 1.44 and 1.43 (*CGS*), respectively). The differences in the first-order transition (in this case, FM↔AFM) appear again [3]. We note that the large signal associated with the second-order phase transition in the as-prepared sample (T_N=136.5 K), which is also observed in the x=0.15 sample

[3] T_t=105.2/107.2 K for as-cast sample and T_t=98.0/99.0 K for T4-annealed samples, on cooling/heating.

(see Fig. 3.7), is strongly reduced when the sample is heat-treated (T_N=131.4 K, see inset in Fig. 3.9), in concordance with the fact that a more correlated system yields a lower ac signal. The large signal of the second-order transition extends over a range ~125-~180 K, it shows differences in the susceptibility depending on the frequency and whether we are cooling or heating, and it shows more than one peak. These effects are caused by the presence of FM clusters both in the AFM phase below T_N and in the PM phase above T_N, fact that is extensively studied in Chapter 8.

It is thus confirmed in both compositional regions that the T4 heat treatment improves the magnetic structure and sharpens the transitions in all samples, although magnetisation measurements at low$T$ showed a slight damage in the latter.

3.2.3 Differential Scanning Calorimetry

Differential scanning calorimetry (DSC)[4] is the most suitable method to study first-order phase transitions since it measures the heat flow, so that a proper integration of the calibrated signal yields the latent heat and the entropy change at the transition [22]. In contrast, ac, relaxation and adiabatic calorimetry -the latter commonly used for the study of MCE [23]- are suitable for determining the heat capacity C_P and they are thus well adapted for studying continuous second-order phase transitions. It should be noted that in a first-order transition, the experimental determination of C_P is intrinsically uncertain due to the release of latent heat [24]. Moreover, a heat input does not result in a modification of the temperature of the sample and, accordingly, ac, relaxation and adiabatic techniques are not suitable for studying first-order phase transitions.

Therefore, DSC measurements were used to characterise the first-order transition in $Gd_5(Si_xGe_{1-x})_4$ alloys for $x \leq 0.5$, and check the effect of the heat treatments on the transition. DSC measures the heat flow, $\dot{Q}(t)$, either released or absorbed by a sample, through a sensor (battery of thermocouples) which furnishes an electrical voltage that is proportional to $\dot{Q}$. Another sensor, with a sample of reference[5] mounted on top, is connected differentially to the former. This enables to minimise any drift caused by changes in the temperature of the calorimetric block, which is continuously scanned with time. $T(t)$ of the block is then measured by a carbon-glass resistor. This enables to compute numerically the heating/cooling rate, dT/dt, and $dQ/dT=\dot{Q}\ (dT/dt)^{-1}$ is thus obtained. The T-integration of the peak in dQ/dT, which appears only at the first-order transition,

[4]DSC is extensively described in Chapter 4.

[5]A material without transitions in the measuring temperature range.

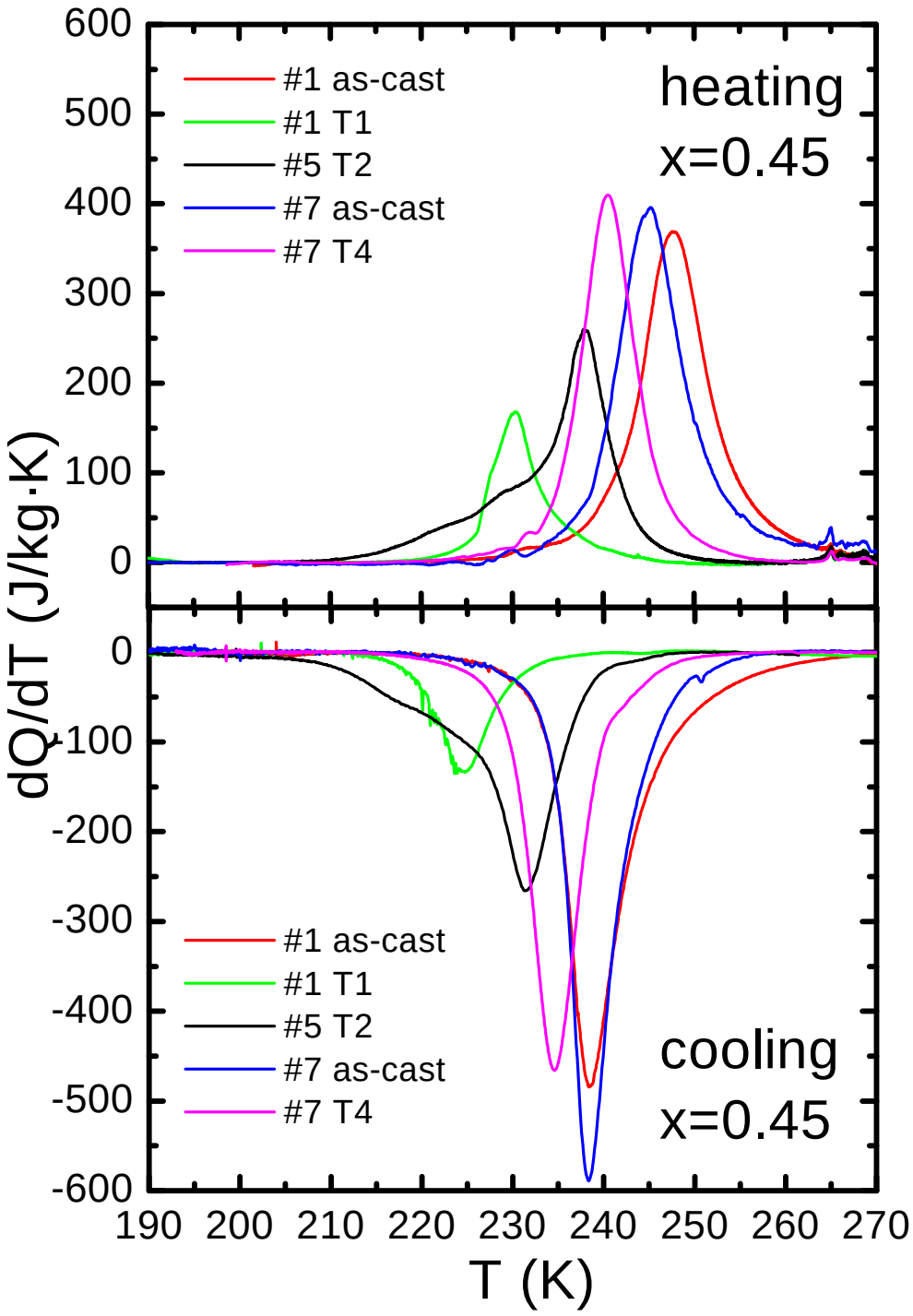

Figure 3.10: DSC data for different samples of x=0.45 compound, with various heat treatments.

x	ID	Heat T.	T_t (K) cool.	heat.	T_N (K)	ΔS (J/kgK) cooling	heating
0.45	#1	NO	238.0	248.0		-19.95	16.55
		T1	224.7	230.5		-8.64	11.72
	#5	T2	230.9	237.8		-12.82	12.38
	#7	NO	238.1	245.0		-17.6	17.0
		T4	232.2	240.0		-18.2	16.9
0.365	#1	NO	195.0	200.0		-30.0	27.42
		T1	~177	~181		Not integrable	
	#2	T2	174.3	177.3		-19.63	21.28
	#3	NO	198.0	207.9		-27.5	25.5
0.3	#2	NO	165.8	175.1		-32.1	30.9
0.25	#2	NO	139.3	149.8		-39.5	37.4
0.2	#1	NO	105.3	119.3	~128	-36.3	38.2
0.18*	#1	NO	98.3	112.8	~127	-29.7	28.8
		T4	93.0	105.5	~128	-25.7	21.4
0.15*	#1	NO	~90	~94	~128	Not integrable	
		T1	-	-	~133	Not integrable	

Table 3.4: Entropy change, ΔS, and temperature of the first-order transition, T_t, obtained from DSC in all measured samples, on cooling and heating. T_N for the corresponding samples is also displayed. *T_t in these samples is close to LN_2 temperature (77 K) and the complete integration of the transition is difficult to obtain.

yields the value of the latent heat (L) and the entropy change (ΔS):

$$L = \int_{T_L}^{T_H} \frac{dQ}{dT} dT \;\; ; \;\; \Delta S = \int_{T_L}^{T_H} \frac{1}{T} \frac{dQ}{dT} dT \;\; , \tag{3.9}$$

where T_H and T_L are respectively temperatures above and below the starting and finishing transition temperatures. The temperature of the first-order phase transition, T_t, may be evaluated as the temperature at the maximum of the dQ/dT peak. Our home-made calorimeter operates over a temperature range from 77 K (LN_2) to 340 K (electrical heater) and has an accuracy of 5-10%.

All measurements, carried out for a variety of samples and annealings, from x=0.15 to x=0.45 (compositions with T_t within the 77-340 K temperature range) are compiled in Table 3.4. Samples with T_t closer to 77 K (x=0.15 and 0.18) show problems since dQ/dT cannot be entirely integrated. Moreover, the second-order

transition, which is shown as a λ-peak in dQ/dT curve, influences the baseline of the first-order peak in x=0.18.

The behaviour of the first-order phase transition and the related entropy change obtained by DSC measurements as a function of heat treatment, can be summarised in Fig. 3.10 for the x=0.45 compound, which reproduces the main results obtained for the whole compositional range $0 \leq x \leq 0.5$. First, two different as-cast samples (#1 and #7) are displayed in Fig. 3.10 in order to check the reproductivity of the features of x=0.45. Both samples yield the same ΔS values and similar T_t, with sligth different hysteresis (see Table 3.4 and Fig. 3.10). T1 heat treatment for sample #1 shifts T_t to lower temperatures (by ~13-18 K) and, although thermal hysteresis is reduced, entropy change is reduced~40-60%. This proves that a large part of the $Gd_5(Si,Ge)_4$ (5:4) structure is transformed into a new phase by T1 annealing. The fact that ΔS largely decreases suggests that these undesired new phases do not show giant MCE. Besides, for x=0.365 (#1) sample, the first-order transition is seriously affected and dQ/dT peak cannot be properly integrated (see Table 3.4). T2 treatment for x=0.45 shifts T_t by ~7-11 K to lower T and the entropy change is reduced ~30%. The latter value agrees with that obtained from magnetisation measurements, giving further evidence that T2 annealing also transforms part of the 5:4 structure. Finally, the T4 heat treatment for sample x=0.45 (#7) decreases T_t by ~5-6 K, narrows the width of the first-order peak (*i.e.*, transition is narrowed because the spread in the x value is reduced) and yields the same values of ΔS as the non-treated sample, proving that this annealing procedure is the most suitable for our samples, in agreement with high field $M(H)$ and ac susceptibility.

3.2.4 X-Ray Diffraction

The detailed determination of the crystallographic structure is relevant for the understanding of the magnetic behaviour in $Gd_5(Si_xGe_{1-x})_4$ alloys (section 2.4). Here we present X-ray diffraction (XRD) for x=0.5, x=0.3, x=0.2, x=0.1 and x=0 as examples for the two compositional regions, and x=0.45 samples with different heat treatments to show the effect of the latter.

x=0.5 (#0) as-cast sample was analysed by XRD and it is shown as an example of the $0.24 \leq x \leq 0.5$ compositional range. Diffraction over the upper sides of the original as-cast button (with characteristic plate-like shaped -faceted-crystalls on the surface) showed a strong texture. The sample was cut into slices, one of them was measured, and still showed texture. Therefore, powder XRD was performed to obtain all reflections of the structure of the alloy. The new powder diffractogram, which was fitted using the Rietveld refinement program FULLPROF [25], is displayed in Fig. 3.11. The lattice and atomic parameters determined in Ref. [21] were used as starting points. Refinement with the mono-

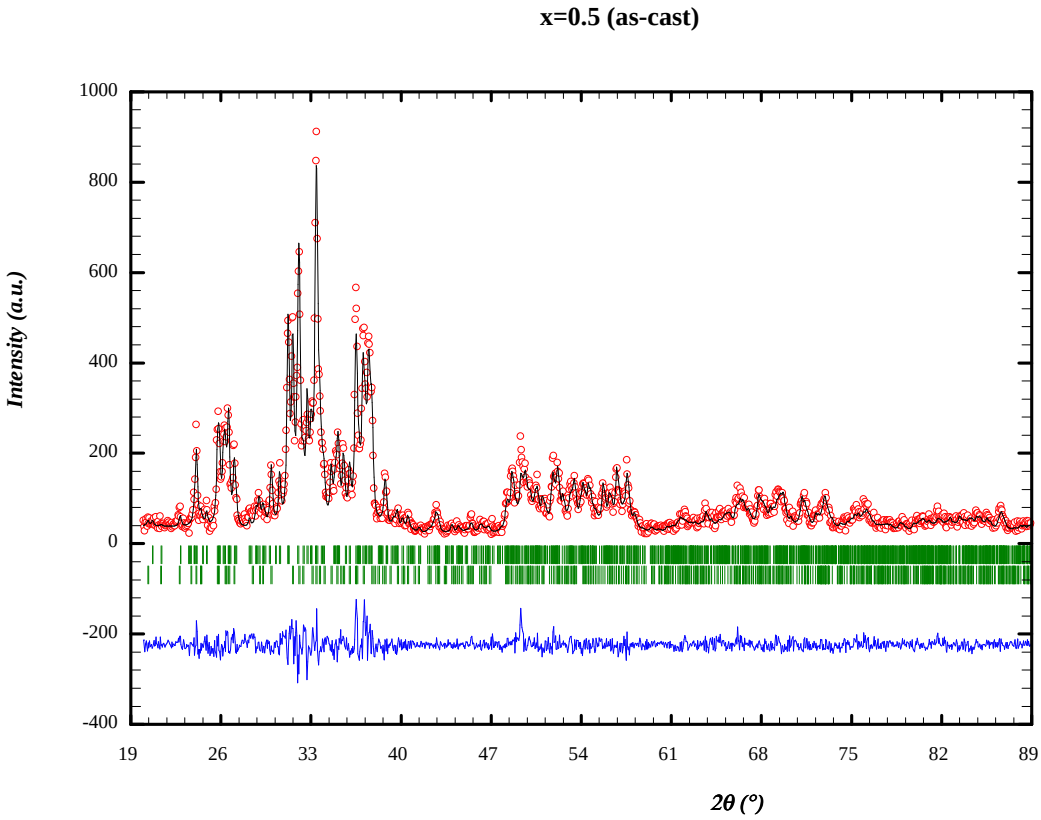

Figure 3.11: XRD data for an as-cast sample of the x=0.5 compound. Open circles correspond to experimental data, while the solid line corresponds to the best fit of the spectra with two phases: one major phase corresponding to the expected monoclinic phase of the x=0.5 compound and one minor orthorhombic phase corresponding to an alloy with x~0.55. Vertical lines show the Bragg positions (those close to the spectra are for x=0.5, those further apart are for a compound with x~0.55) and the bottom solid line is the difference between experimental and fitted data.

$Gd_5(Si_xGe_{1-x})_4$ x=0.5				
space group	a (Å)	b (Å)	c (Å)	γ (º)
$P112_1/a$	7.577(1)	14.790(3)	7.779(1)	93.09(1)
atom	x/a	y/b	z/c	occupancy
Gd1 in 4(e)	0.320(4)	0.251(1)	-0.002(3)	1
Gd2a in 4(e)	-0.001(3)	0.095(1)	0.184(1)	1
Gd2b in 4(e)	0.019(3)	0.398(1)	0.181(3)	1
Gd3a in 4(e)	0.357(3)	0.886(1)	0.176(3)	1
Gd3b in 4(e)	0.330(3)	0.619(1)	0.175(1)	1
M1 in 4(e) (T)	0.223(6)	0.251(3)	0.379(6)	0.6(1)
M2 in 4(e) (T)	0.97(1)	0.247(6)	0.91(1)	0.6(1)
M3a in 4(e) (T')	0.213(7)	0.965(3)	0.514(6)	0.4(1)
M3b in 4(e) (T')	0.151(7)	0.565(3)	0.502(6)	0.4(1)
$Gd_5(Si_xGe_{1-x})_4$ x~0.55				
space group	a (Å)	b (Å)	c (Å)	γ (º)
Pnma	7.510(1)	14.779(3)	7.802(2)	90
atom	x/a	y/b	z/c	occupancy
Gd1 in 4(c)	0.344(4)	1/4	0.016(3)	0.5
Gd2 in 8(d)	0.023(2)	0.0992(8)	0.178(2)	1
Gd3 in 8(d)	0.323(2)	0.8775(9)	0.176(2)	1
M1 in 4(c) (T)	0.204(5)	1/4	0.371(7)	0.02(6)
M2 in 4(c) (T)	0.959(8)	1/4	0.913(8)	0.14(6)
M3 in 8(d) (T')	0.171(7)	0.955(2)	0.472(6)	0.42(7)

Table 3.5: Space group, cell parameters, atomic sites and occupancy for the two phases present in the as-cast x=0.5 sample. M stands for the atomic sites occuped by a mixture of Si and Ge atoms. T and T' sites are explained in section 2.3. In this table only Si occupations are listed for M positions.

clinic structure (space group $P112_1/a$) did not account for all reflections present in the experimental diffractogram. The existence of a secondary phase with $x>0.5$, which has an orthorhombic structure (space group *Pnma*), was thus assumed [1]. With this second phase all the remaining reflections were fitted. Table 3.5 displays all refined structural parameters. The obtained values are consistent with those given in literature [21, 26] and allow to estimate x of the second phase as ~0.55 (in good agreement with Ref. [21]). Some preferential orientation (~17 %) still exists along the (0 1 0) direction. The percentage of the secondary phase reaches 40% mol. This high value is easily understood by taking into account a very recent result for $x\cong0.5$ compounds [7, 5, 6]: a polymorphism between *M* and *O*(*I*) phases occurs depending on the temperature that the sample reaches in the melting and/or posterior annealing (section 2.2). Therefore, both phases -*M* and *O*(*I*)- are typical of $x\cong0.5$ alloys. It is worth noting that occupancy of Si and Ge atoms is not equiprobable, but there are preferences depending on the atomic sites, as discussed in Refs. [26, 27]. The study of a monocrystal with x=0.5 showed that T sites (intraslab) are preferably occuped by Si (60%), while the occuppancy in T' sites (interslab) is 60% Ge and 40% Si [26]. In our polycrystalline sample, we obtain the same occupancy for the main monoclinic phase (see Table 3.5). The other samples with the same compositional region, x=0.3 (#2 as-cast) and x=0.45 (#7 as-cast) also show the monoclinic structure, with a residual phase (~10% mol.) that we have indentified and indexed as Ge-rich Gd(Si,Ge) (BCr-type orthorhombic structure, *Cmcm* space group).[6] x=0.45 as-cast sample also presents a secondary phase corresponding to a 5:4 phase with $x>0.5$, *i.e.*, with *O*(*I*) structure. The cell parameters of the analysed samples are displayed in Table 3.7). With these secondary phases all remaining reflections were fitted.

As a paradigmatic example of the Ge-rich compositional region ($0 \leq x \leq 0.2$), the x=0.1 compound (#1 as-cast) is presented. The sample was powdered in order to get the diffractogram, which is shown in Fig. 3.12. The expected *Pnma* space group (orthorhombic structure) was found. The lattice and atomic parameters determined in Ref. [2] were used as starting points. Minor amounts of residual phases were detected and indexed as Ge-rich Gd(Si,Ge) (~10% mol.) and $Gd_5(Si,Ge)_3$ (~5% mol., $P6_3/mcm$ space group with Mn_5Si_3-type hexagonal structure).[7] The refined unit-cell parameters and atomic positions are displayed in Table 3.6. x=0 (#1 and #3) and x=0.2 (#1) as-cast samples yield similar results, although for the latter only Gd(Si,Ge) is detected as residual phase (~10% mol.). Table 3.7 compiles the space group, cell parameters and residual phases for the

[6] GdSi shows a BFe-type orthorhombic structure (*Pnma*), which is different from that of GdGe. The identified secondary 1:1 phase presents the GdGe structure with lower lattice parameters, indicating the presence of Si in the structure.

[7] In this case, Gd_5Si_3 and Gd_5Ge_3 show the same structure, with larger lattice parameters for the latter compound.

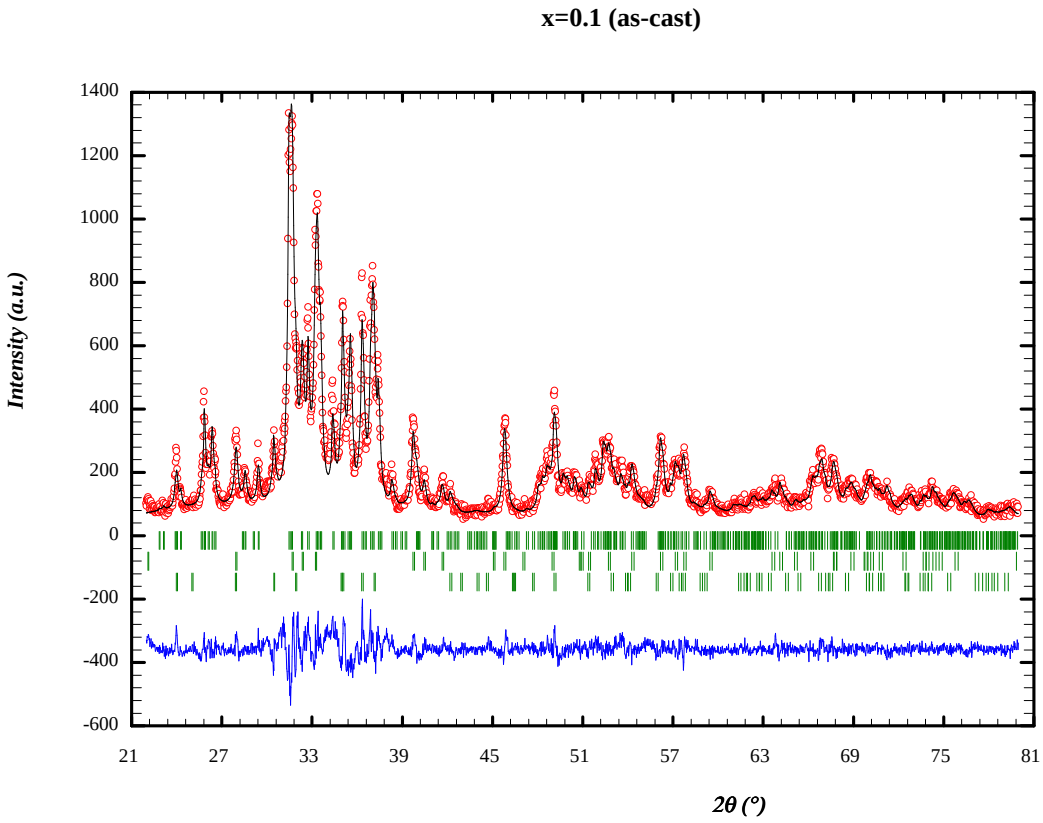

Figure 3.12: XRD data for an as-cast sample of the x=0.1 compound. Open circles correspond to experimental data, while the solid line corresponds to the best fit of the spectra with three phases: one major phase corresponding to the expected orthorhombic phase of the x=0.1 compound and two minor phases corresponding to 1:1 [Gd(Si,Ge)] and 5:3 [$Gd_5(Si,Ge)_3$] compounds. Vertical lines show the Bragg positions (for 5:4, 1:1 and 5:3 phases, from top to bottom) and the bottom solid line is the difference between experimental and fitted data.

$Gd_5(Si_xGe_{1-x})_4$ x=0.1				
space group	a (Å)	b (Å)	c (Å)	γ (º)
Pnma	7.683(2)	14.824(3)	7.778(2)	90
atom	x/a	y/b	z/c	occupancy
Gd1 in 4(c)	0.296(2)	1/4	-0.005(2)	0.5
Gd2 in 8(d)	-0.014(1)	0.1009(7)	0.194(2)	1
Gd3 in 8(d)	0.382(1)	0.8806(7)	0.164(2)	1
M1 in 4(c) (T)	0.160(4)	1/4	0.354(4)	0.05
M2 in 4(c) (T)	0.901(5)	1/4	0.909(4)	0.05
M3 in 8(d) (T')	0.228(3)	0.956(3)	0.485(3)	0.1
Gd(Si,Ge)				
space group	a (Å)	b (Å)	c (Å)	γ (º)
Cmcm	4.330(1)	10.770(3)	3.959(1)	90
$Gd_5(Si,Ge)_3$				
space group	a (Å)	b (Å)	c (Å)	γ (º)
$P6_3/mcm$	8.547(2)	8.547(2)	6.376(2)	120

Table 3.6: Space group, cell parameters, atomic sites and occupancy for as-cast x=0.1 sample. M stands for the atomic sites occuped by a mixture of Si and Ge atoms. T and T' sites are explained in section 2.3. In this table only Si occupations are listed for M positions. Space group and cell parameters for secondary phases are included.

$Gd_5(Si_xGe_{1-x})_4$						
x	space group	a (Å)	b (Å)	c (Å)	γ (º)	Sec. phases
0	*Pnma*	7.7010(8)	14.832(2)	7.7896(9)	90	1:1, 5:3
0.1	*Pnma*	7.683(2)	14.824(3)	7.778(2)	90	1:1, 5:3
0.2	*Pnma*	7.676(1)	14.817(2)	7.772(1)	90	1:1
0.3	$P112_1/a$	7.622(2)	14.826(4)	7.780(2)	92.93(2)	1:1
0.45	$P112_1/a$	7.5896(8)	14.810(2)	7.7846(9)	93.123(7)	1:1, x>0.5
0.5	$P112_1/a$	7.577(1)	14.790(3)	7.779(1)	93.09(1)	x~0.55

Table 3.7: Space group, cell parameters and secondary phases for various $Gd_5(Si_xGe_{1-x})_4$ as-cast alloys, obtained from XRD data.

analysed compounds, being in good agreement with Ref. [21]. We note that all compositions except for x=0.5 present the 1:1 phase. This phase is GdGe-based (a= 4.339(4) Å, b = 10.79(2) Å and c = 3.973(4) Å[28]), but the decreasing of the refined cell parameters with x suggests that it is doped with Si, see Table 3.8. With these secondary phases all remaining reflections were fitted.

Finally, X-ray powder diffraction was carried out in different parts of x=0.45 (#7) sample, with no heat treatment, T4 treatment and T4+quenching (see Fig. 3.13), in order to prove the effect of annealing on the crystallographic structure of the samples. The three diffractograms showed the same characteristics (main phase being monoclinic with space group $P112_1/a$) with only slight differences in the intensity of some reflection peaks, which correspond to minor amonts of residual phases. Some of these peaks increased from the as-cast sample to the quenched one, corresponding to Gd(Si,Ge) phase and proving that the heat treatment favours the segregation of secondary phases. Other peaks, corresponding to the $O(I)$ structure of the 5:4 phase with x>0.5, decreased with the heat treatments.

To conclude, XRD enables us to show that samples synthesized with the arc-melting furnace present the expected crystallographic structures, which depends on the compositional region of $Gd_5(Si_xGe_{1-x})_4$ alloys system. T4 heat treatment and posterior quenching maintains the crystallographic structure of the samples and homogenises the x value of the 5:4 main phase, although they favour the segregation of the secondary phases already present in the as-cast samples.

Gd(Si,Ge)				
Main phase (x)	space group	a (Å)	b (Å)	c (Å)
0	*Cmcm*	4.386(2)	10.676(3)	3.981(2)
0.1	*Cmcm*	4.330(1)	10.770(3)	3.959(1)
0.2	*Cmcm*	4.328(1)	10.758(3)	3.943(1)
0.3	*Cmcm*	4.329(1)	10.735(3)	3.9393(8)
0.45	*Cmcm*	4.328(1)	10.719(2)	3.916(1)

Table 3.8: Space group and cell parameters for secondary 1:1 phases present in various $Gd_5(Si_xGe_{1-x})_4$ as-cast alloys, obtained from XRD data.

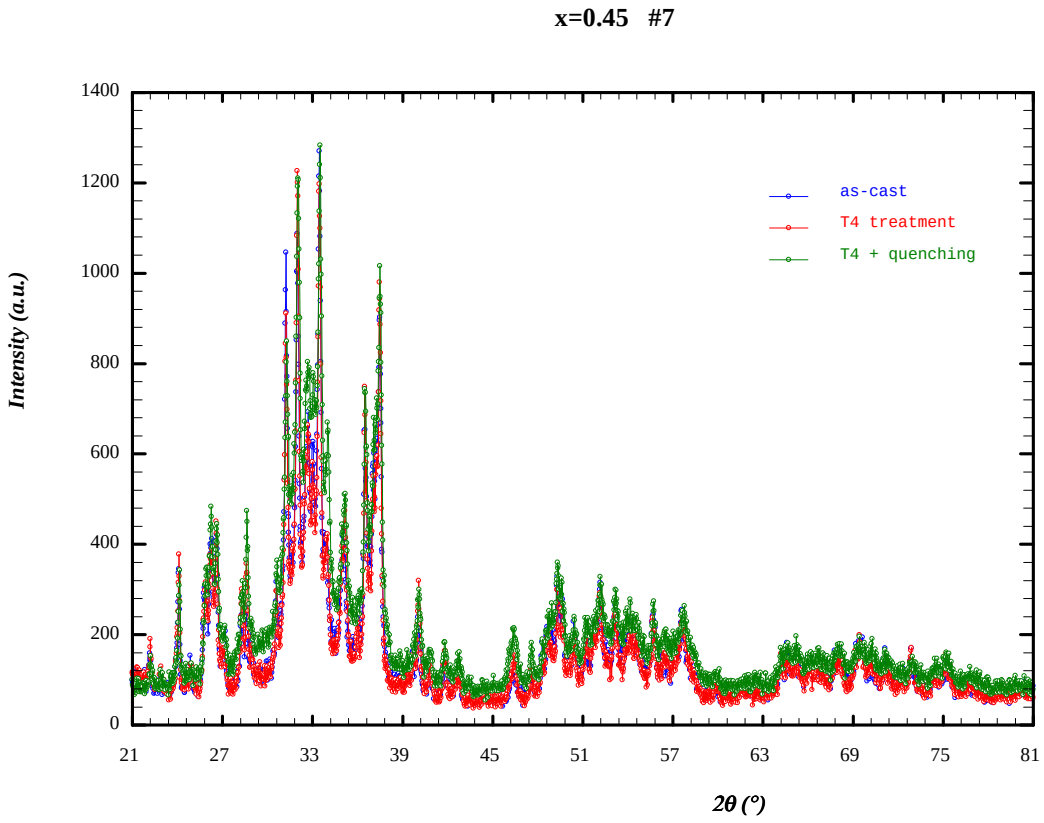

Figure 3.13: XRD data for x=0.45 samples with different annealings.

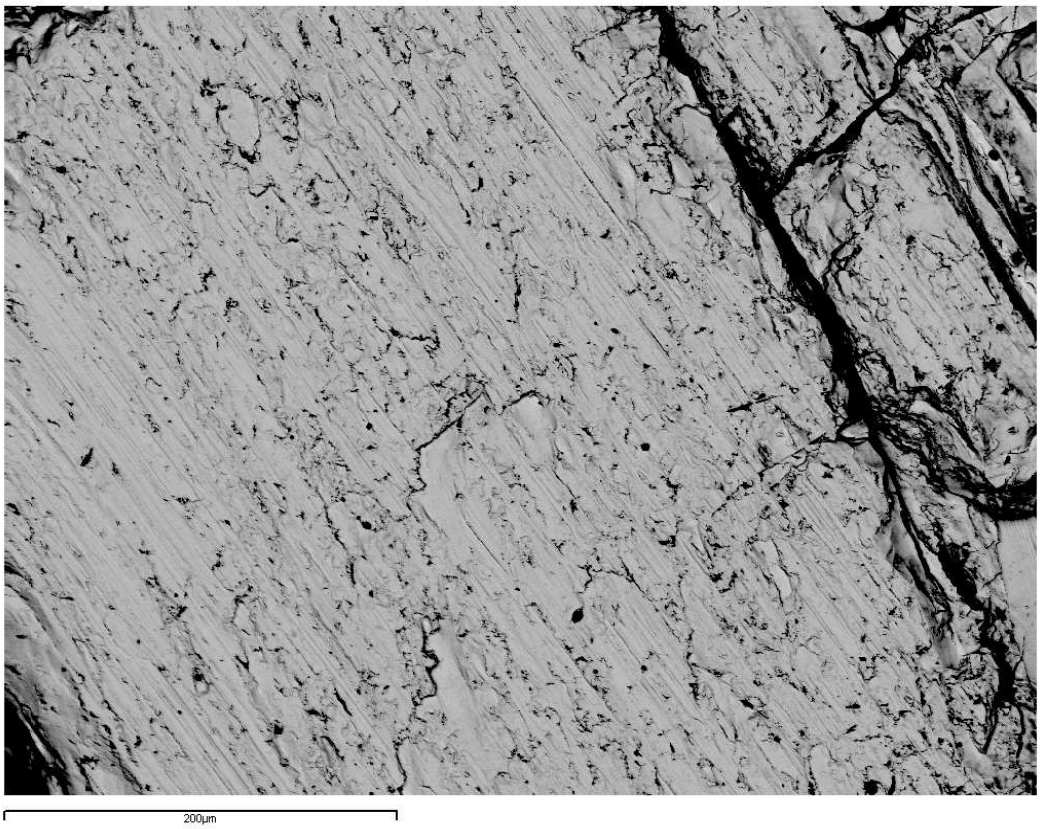

Figure 3.14: Secondary electron image, obtained with SEM, of the surface of a x=0 as-cast sample (#1).

3.2.5 Scanning Electron Microscopy (SEM) and Electron-beam Microprobe

Some samples were analysed by SEM in order to image the different phases present. These phases were studied by Energy Dispersive Spectroscopy (EDS), which is incorporated in the SEM system itself. Different phases in the sample with x=0 were difficult to observe due to the presence of microcracks in the surface, since Ge-rich alloys are more brittle than Si-rich ones (see Fig. 3.14). EDS found only the main 5:4 phase in the various regions of the sample. Heat-treated (T4) sample with x=0.45 showed a more polished surface and a backscattered electron image unveiled four different phases (dark grey, middle grey, light grey and middle-grey lines in Fig. 3.15). The various phases were difficult to differentiate, since 5:4, 5:3 and 1:1 phases are close in composition.

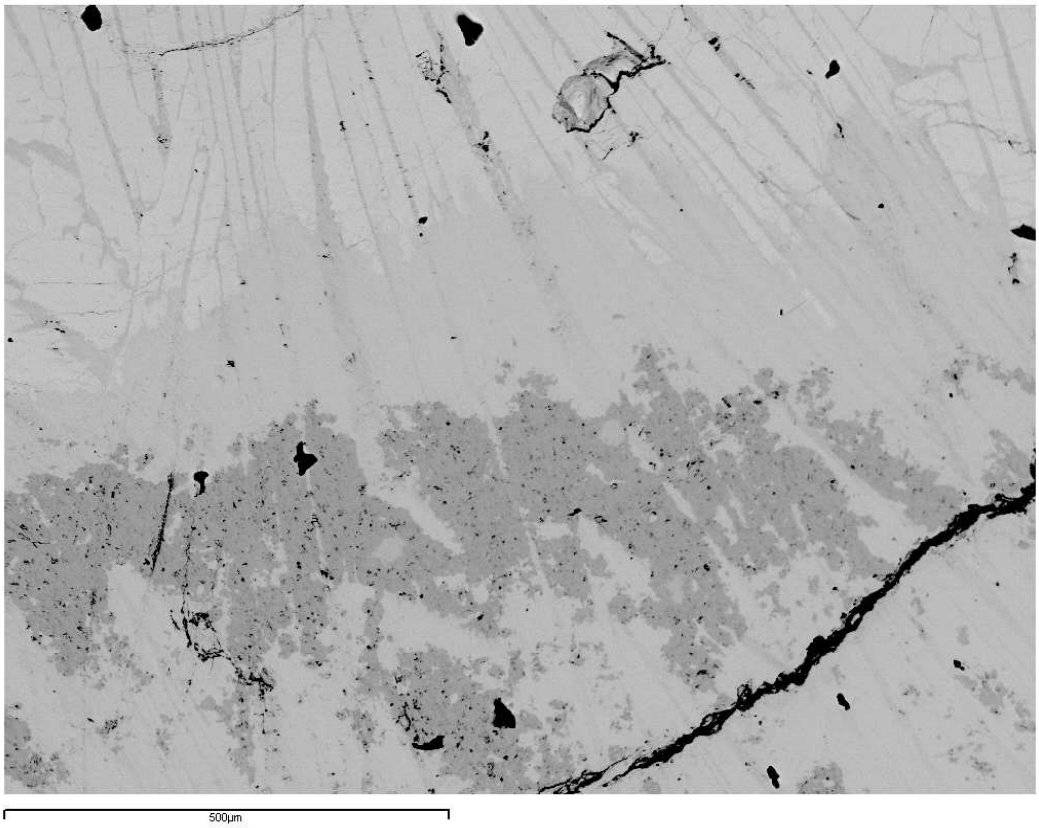

Figure 3.15: Backscattered electron image, obtained with SEM, of the surface of a x=0.45 T4-treated sample (#7).

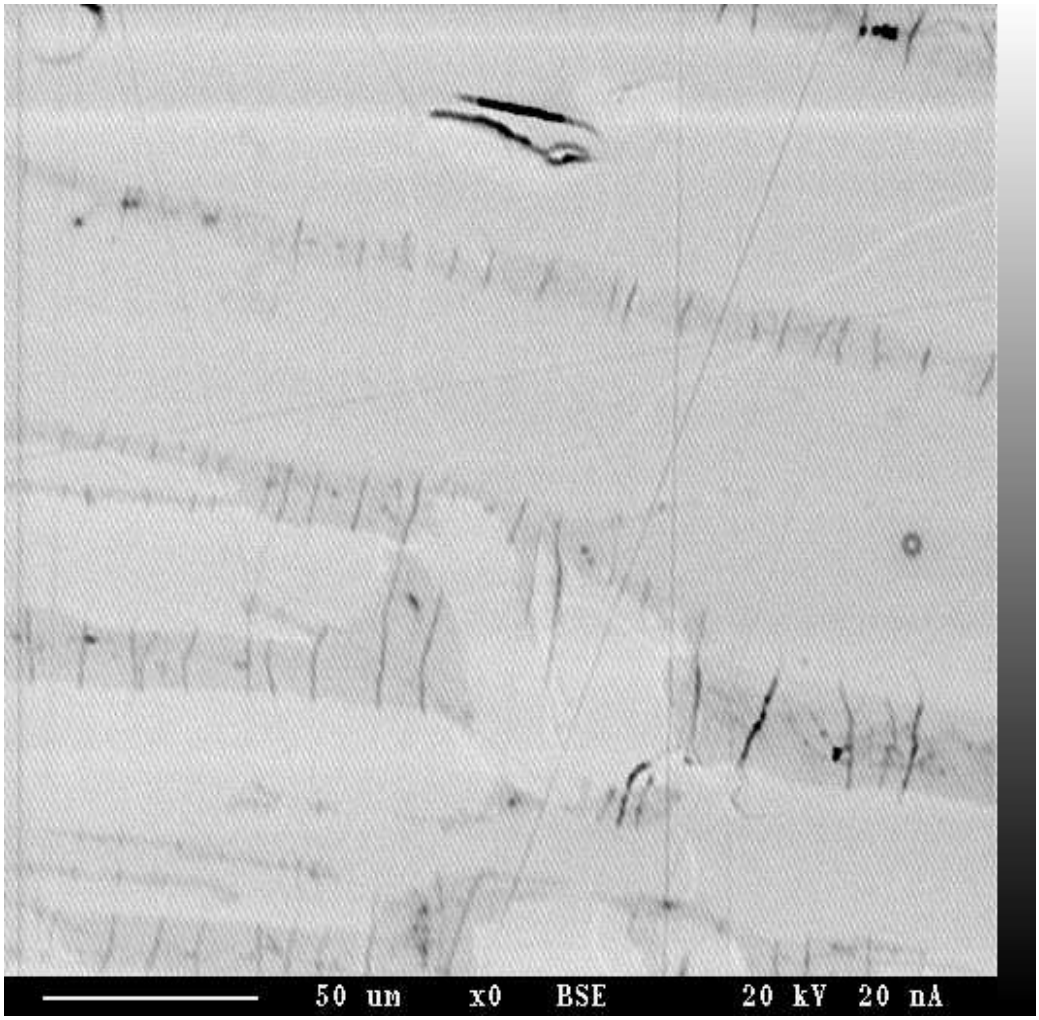

Figure 3.16: Backscattered electron image, obtained with the SEM of a microprobe, of the surface of x=0 as-cast sample (#1).

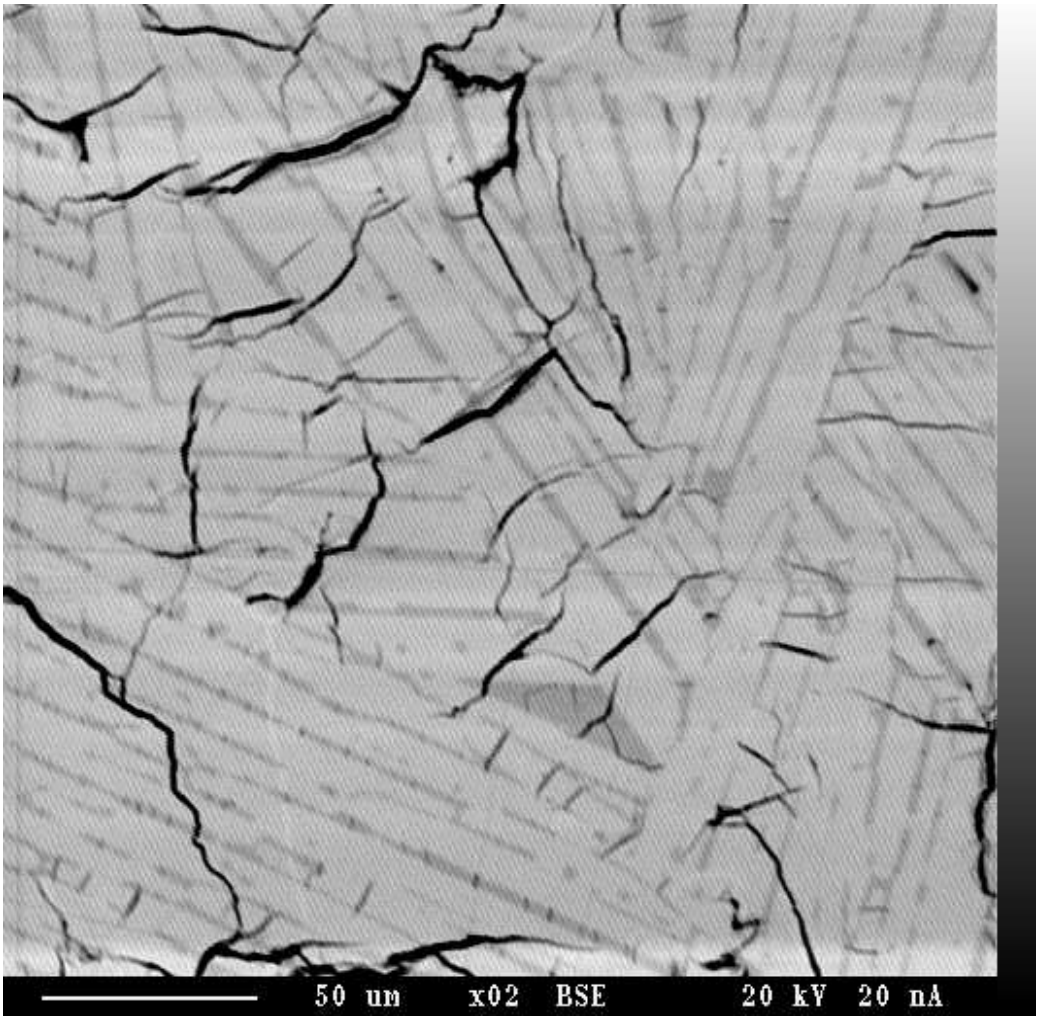

Figure 3.17: Backscattered electron image, obtained with the SEM of a microprobe, of the surface of x=0.2 as-cast sample (#1).

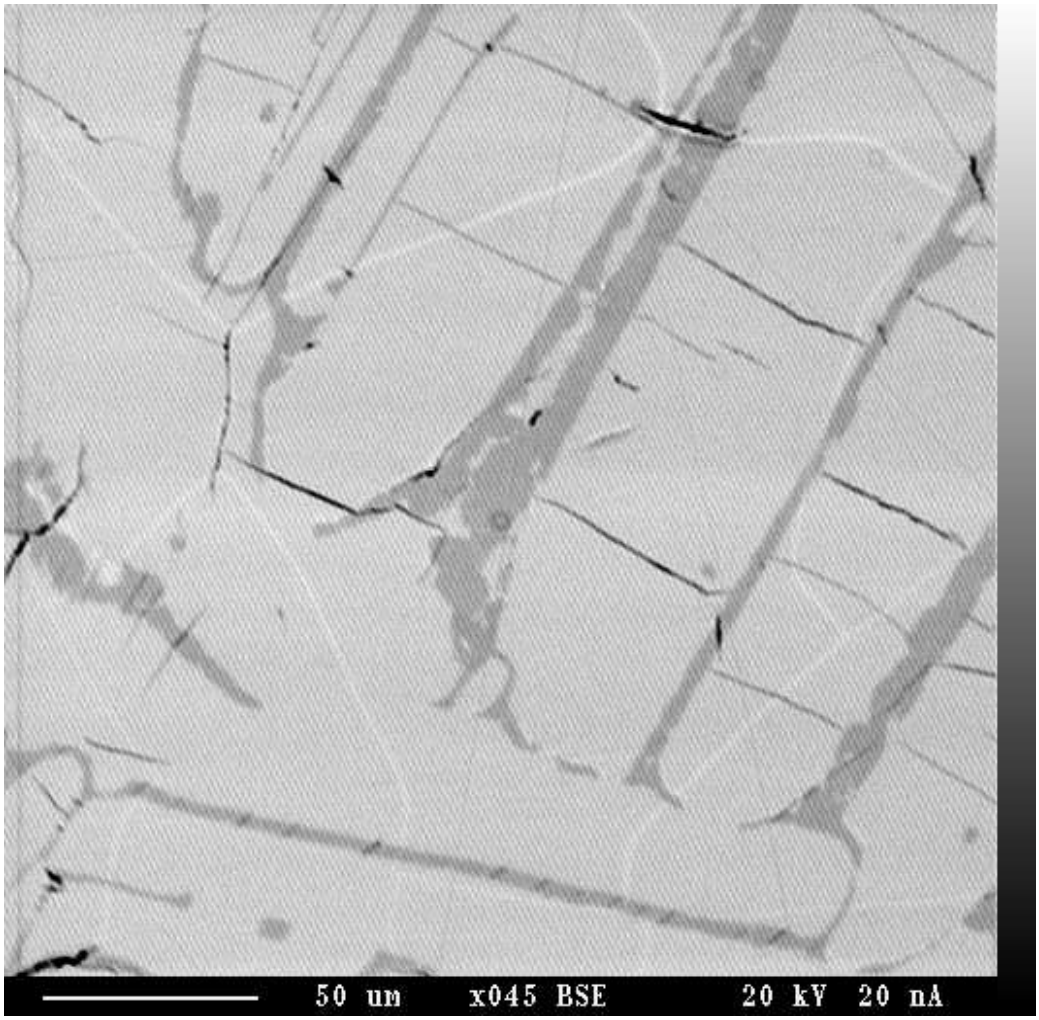

Figure 3.18: Backscattered electron image, obtained with the SEM of a microprobe, of the surface of x=0.45 as-cast sample (#7).

For this reason an electron-beam microprobe -with Wavelenght Dispersive Spectroscopy (WDS)- was used due to its higher resolution. A variety of samples (x=0 #1 as-cast, x=0.2 #1 as-cast, x=0.45 #7 as-cast and T4-treated) were properly prepared, with a gold deposition on top, to be analysed with the microprobe. For x=0, althought different tones could be identified in a backscattered electron image (see Fig. 3.16), WDS analysis yielded the same 5:4 phase (being 55.8% at. Gd for the main light grey phase and 54.2% at. Gd for the dark-grey lines). Taking into account the latter result and that the 5 K magnetisation in this sample is saturated at relatively low field (as compared with the other samples, see Fig. 3.1) -yieding a saturation magnetisation similar to other reported values and higher than the theoretical 7.0 μ_B- the secondary phases detected by XRD in this sample are indeed residual. For x=0.2, the main observed phase corresponded to the 5:4 phase with x=0.197, *i.e.*, the nominal stochiometric value. A pattern of dark lines is observed in the backscattered electron image of this sample (see Fig. 3.17), which appears to be a 5:4 phase with x=0.158. This secondary phase is not observed in XRD, probably because it presents the same crystallographic structure ($O(I)$) and the x value is close to the value of the main phase, which just yields broader peaks in the diffractogram. For x=0.45 as-cast sample, the main observed phase also corresponded to the 5:4 phase, with x=0.413, which is slightly lower than the nominal value. A pattern of dark lines is also observed in the backscattered electron image of the sample (see Fig. 3.18), and in this case the WDS analysis yielded a 5:4 phase with x=0.509, in agreement with the value estimated from the anomaly in the ac susceptibility at T=294.5±0.5 K (~0.51-0.53). Finally, the same x=0.45 sample, heat-treated, was analysed (Fig. 3.15). The dark-grey phase corresponds to a 2:3 phase, which is present in the Gd-Ge phase diagram, close to the 1:1 phase, but not in the Gd-Si one (see Figs. 3.3 and 3.4). The middle-grey phase, surrounding the dark-grey phase, corresponds to the 1:1 phase, with a Si/Ge ratio of x=0.40. The light-grey phase is the main phase, with 5:4 ratio between Gd and Si/Ge. In this phase, the ratio between Si and Ge is x=0.415, which is very close to the value observed in the as-cast sample. The pattern of dark lines, crossing the rest of phases, is still observed. The WDS analysis of these lines yields a 5:4 phase with x=0.460. This is in agreement with the observation in ac susceptibility, in which the anomaly related to the residual phase with x>0.5 disappeared after the heat treatment. The segregation of phases with ratio different from 5:4 during the heat treatment is evident from SEM images and electron-beam Microprobe analysis, as already suggested from other experimental techniques. We point out that the 2:3 phase, which was not detected using XRD patterns, is a very poorly studied phase and almost no literature is available.

3.3 Conclusions

All techniques show that our home-made arc-melting furnace synthesizes $Gd_5(Si_xGe_{1-x})_4$ samples of the desired stochiometry. SEM and microprobe analyses show that the main 5:4 phases with the desired x are obtained. Ac susceptibility shows the magnetic transitions occurring in these alloys, while XRD detects the crystallographic structures corresponding to the phases at room temperature. $M(H)$ at 5 K shows the presence of secondary amounts of Gd(Si,Ge) (1:1) and $Gd_5(Si,Ge)_3$ (5:3) phases in all samples. This presence is confirmed by XRD and microprobe analyses, which also detect residual 5:4 phases with an x value different from that of the main phase. DSC shows that all samples present the first-order transition, and that secondary phases do not affect the latter. Heat treatments favour the segregation of these secondary phases ($M(H)$, XRD, SEM and microprobe), but also reduce the spread in the x value (ac susceptibility and DSC) and removes 5:4 residual phases with very different x values (as susceptibility and microprobe). Therefore, a trade-off between phase segregation and removal of x spread is needed. T4 and T4 + quenching treatments enable such a trade-off.

Bibliography

[1] L. Morellon, P. A. Algarabel, M. R. Ibarra, J. Blasco, B. García-Landa, Z. Arnold, and F. Albertini, Phys. Rev. B **58**, R14721 (1998).

[2] L. Morellon, J. Blasco, P. A. Algarabel, and M. R. Ibarra, Phys. Rev. B **62**, 1022 (2000).

[3] J. S. Meyers, S. Chumbley, F. Laabs, and A. O. Pecharsky, Scripta Mater. **47**, 509 (2002).

[4] C. Magen, L. Morellon, P. A. Algarabel, C. Marquina, and M. R. Ibarra, J. Phys.: Condens. Matter **15**, 2389 (2003).

[5] V. K. Pecharsky, A. O. Pecharsky, and K. A. Gschneidner, Jr., J. Alloys Comp. **344**, 362 (2002).

[6] V. K. Pecharsky, G. D. Samolyuk, V. P. Antropov, A. O. Pecharsky, and K. A. Gschneidner, Jr., J. Solid State Chem. **171**, 57 (2003).

[7] A. O. Pecharsky, V. K. Pecharsky, and K. A. Gschneidner, Jr., J. Appl. Phys. **93**, 4722 (2003).

[8] J. S. Meyers, S. Chumbley, F. Laabs, and A. O. Pecharsky, Acta Mater. **51**, 61 (2003).

[9] E. M. Levin, K. A. Gschneidner, Jr., and V. K. Pecharsky, Phys. Rev. B **65**, 214427 (2002).

[10] V. K. Pecharsky and K. A. Gschneidner, Jr., Adv. Cryog. Eng. **43**, 1729 (1998).

[11] E. M. Levin, V. K. Pecharsky, and K. A. Gschneidner, Jr., Phys. Rev. B **62**, R14625 (2000).

[12] E. M. Levin, V. K. Pecharsky, and K. A. Gschneidner, Jr., J. Magn. Magn. Mater. **231**, 135 (2001).

[13] L. D. Tung, K. H. J. Buschow, and J. J. M. F. N. P. Thuy, J. Magn. Magn. Mater. **154**, 96 (1996).

[14] F. Canepa, S. Cirafici, and M. Napoletano, J. Alloys Comp. **335**, L1 (2002).

[15] K. H. J. Buschow, Rep. Prog. Phys. **42**, 1373 (1979).

[16] E. C. Stoner, Philos. Mag. **36**, 803 (1945).

[17] D. X. Chen, J. A. Brug, and R. B. Goldfarb, IEEE Trans. Magn. **27**, 3601 (1991).

[18] A. H. Morrish, *The Physical Principles of Magnetism* (Wiley, New York, 1965), Chap. 1.

[19] V. K. Pecharsky and K. A. Gschneidner, Jr., Appl. Phys. Lett. **70**, 3299 (1997).

[20] E. M. Levin, V. K. Pecharsky, K. A. Gschneidner, Jr., and P. Tomlinson, J. Magn. Magn. Mater. **210**, 181 (2000).

[21] V. K. Pecharsky and K. A. Gschneidner, Jr., J. Alloys Comp.**260**, 98 (1997).

[22] W. Hemminger and G. Höhne, *Calorimetry. Fundamentals and practice.* (Verlag Chemie, Weinheim, 1984).

[23] V. K. Pecharsky, J. O. Moorman, and K. A. Gschneidner, Jr., Rev. Sci. Instrum. **68**, 4196 (1997).

[24] V. K. Pecharsky and K. A. Gschneidner, Jr., J. Appl. Phys.**86**, 6315 (1999).

[25] J. L. Rodríguez-Carvajal, Physica B **192**, 55 (1992).

[26] W. Choe, V. K. Pecharsky, A. O. Pecharsky, K. A. Gschneidner, Jr., V. G. Young, Jr., and G. J. Miller, Phys. Rev. Lett. **84**, 4617 (2000).

[27] E. M. Levin, A. O. Pecharsky, V. K. Pecharsky, and K. A. Gschneidner, Jr., Phys. Rev. B **63**, 064426 (2001).

[28] A. G. Tharp, G. S. Smith, and Q. Johnson, Acta Crystallogr.**20**, 583 (1966).